

# Effective Magnetic Susceptibility of Dust Grains with Superparamagnetic Inclusions and Implications

THIEM HOANG<sup>1,2</sup>

<sup>1</sup>*Korea Astronomy and Space Science Institute, Daejeon 34055, Republic of Korea*

<sup>2</sup>*Department of Astronomy and Space Science, University of Science and Technology, 217 Gajeong-ro, Yuseong-gu, Daejeon, 34113, Republic of Korea*

(Dated: Draft version February 17, 2026)

## ABSTRACT

Magnetic properties of dust grains play a fundamental role in their alignment with ambient magnetic fields and magnetic dipole emission. In the radiative torque (RAT) paradigm, superparamagnetic inclusions (SPIs) embedded within dust grains are expected to significantly enhance magnetic susceptibility and alignment efficiency. Previous studies have generally assumed SPIs of a single characteristic size. In this work, we develop an effective superparamagnetism model that explicitly accounts for a power-law size distribution of SPIs. We show that the effective zero-frequency susceptibility can be described by the superparamagnetic susceptibility of uniform-sized inclusions evaluated at the critical blocking size, reduced by a factor  $F_{\text{eff}} \sim 0.1$ . It exhibits a slight increase with dust temperature  $T_d$ , in contrast to the rapid decrease for the case of single-size SPIs. For rotating grains at angular frequency  $\omega$ , we identify a characteristic resonance size of SPIs that dominates the magnetic response,  $N_{\text{res}} = (T_d/T_{\text{act}}) \ln(\nu_0/\omega)$  with  $T_{\text{act}}$  activation temperature and  $\nu_0$  the characteristic attempt frequency of SPIs. The frequency-dependent effective susceptibility is well described by the maximum susceptibility  $\chi_{\text{eff}}^{\text{max}}(\omega)$  at  $N_{\text{res}}$ , reduced by a factor  $G_{\text{eff}} \sim 0.1$ . Unlike models assuming uniform-sized inclusions, we find that the effective susceptibility exhibits a nearly flat spectrum for frequency below  $\nu_0$ , arising from the progressive activation of larger inclusions at lower frequencies. This effective superparamagnetism model based on the SPI size distribution has important implications for magnetic grain alignment, dust polarization, and magnetic dipole emission across diverse environments.

## 1. INTRODUCTION

The alignment of non-spherical dust grains with ambient magnetic fields causes the polarization of distant starlight (J. S. Hall 1949; W. A. Hiltner 1949) and polarized thermal dust emission (R. H. Hildebrand 1988; Planck Collaboration et al. 2015). Dust polarization has become one of the primary tools for tracing the magnetic fields (B-fields) projected in the plane of the sky (2D B-fields) across a wide range of astrophysical environments, from the diffuse interstellar medium (ISM) and molecular clouds to star- and planet-forming regions (K. Pattle et al. 2023; Y. Tsukamoto et al. 2023). The polarization degree also provides insight into dust properties (size, shape, and composition) (B. Draine 2024; T. Hoang & B. Truong 2024; B. Truong & T. Hoang 2025), and the physical processes responsible for grain alignment (A. Lazarian 2003; A. Lazarian et al. 2015).

Magnetic properties of dust grains have been recognized as essential for grain alignment with magnetic fields since the earliest theoretical studies of interstellar dust alignment so-called paramagnetic relaxation mech-

anism (L. J. Davis & J. L. Greenstein 1951). Iron, the fifth abundant element in the universe, is heavily depleted from the gas phase, with more than 95% of iron incorporated into dust grains (E. B. Jenkins 2009). While the precise chemical and structural form of iron in dust remains uncertain, in-situ measurements and astronomical modeling suggest that a significant fraction of iron may be present in the form of metallic or iron-oxide clusters embedded within larger silicate grains (J. P. Bradley 1994). Modern dust models, including THEMIS (N. Ysard et al. 2024) and Astrodust (B. S. Hensley & B. T. Draine 2023), incorporate iron inclusions to reproduce observed extinction, emission, and polarization properties.

Incorporation of iron clusters of nanometer-size (hereafter superparamagnetic inclusions–SPIs) into a dust grain can strongly enhance the magnetic response of dust grains, making the composite grain superparamagnetic material. Early works noted that SPIs increase magnetic relaxation rates of rotating grains and thus induce more efficient alignment with magnetic fields (R. V.

Jones & L. Spitzer 1967; J. S. Mathis 1986; P. G. Martin 1995; A. A. Goodman & D. C. B. Whittet 1995). In the Radiative Torque (RAT) paradigm (A. Z. Dolginov & I. G. Mitrofanov 1976; B. T. Draine & J. C. Weingartner 1997; A. Lazarian & T. Hoang 2007; T. Hoang & A. Lazarian 2008), grain alignment depends on three key ingredients: dust properties (including magnetic susceptibility), the radiation field, and local gas conditions (e.g., T. Hoang et al. 2022). Superparamagnetism plays a particularly important role in Magnetically enhanced RAT (MRAT) alignment, where enhanced magnetic relaxation stabilizes high-angular-momentum (high- $J$ ) attractor points and increases alignment efficiency (A. Lazarian & T. Hoang 2008; T. Hoang & A. Lazarian 2016a; A. Lazarian & T. Hoang 2019; T. Hoang 2025). Radiative torques can also induce rotational disruption of dust grains (aka. RATD) due to centrifugal stress when the grain angular velocity exceeds the critical limit determined by the material tensile strength (T. Hoang et al. 2019; T. Hoang 2019). The RATD is an important mechanism that affects the evolution of dust in strong radiation fields, and its efficiency also depends on magnetic properties (T. Hoang 2025).

In addition to alignment, thermal fluctuations of magnetic moments in SPIs produce magnetic dipole emission (MDE), which has been proposed as a potential foreground component of the cosmic microwave background (CMB) (B. T. Draine & A. Lazarian 1999a; T. Hoang & A. Lazarian 2016b). Thus, the magnetic susceptibility of dust grains containing SPIs is fundamental not only for grain alignment but also for MDE.

Despite this importance, previous treatments of superparamagnetism in dust grains have generally assumed SPIs of a single characteristic size when computing magnetic susceptibility and relaxation rates. This simplifying assumption overlooks a crucial physical property: the superparamagnetic relaxation time depends exponentially on inclusion volume. In realistic astrophysical environments, iron clusters are expected to form with a range of sizes. Laboratory experiments demonstrate the formation of iron clusters spanning nanometer scales (C. Davoisne et al. 2006; Z. Djouadi et al. 2007), and theoretical studies suggest that the maximum size of SPIs depends on dust temperature and thermal activation (H. Yang 2021). Because the magnetic response is highly size-sensitive, a distribution of inclusion sizes can fundamentally alter the effective magnetic susceptibility of dust grains.

The size dependence becomes even more critical when considering rotating grains. For a grain rotating at angular frequency  $\omega$ , the magnetic response is frequency dependent, and only SPIs with Néel relaxation times,

which is determined by dust temperature, comparable to  $\omega^{-1}$  contribute efficiently to magnetic response. As a result, the dominant inclusion size depends on both rotation rate and dust temperature. This frequency- and temperature-selective behavior cannot be captured by single-size SPI models. Moreover, while ordinary paramagnetism predicts a Curie-like decrease of static susceptibility with increasing temperature, the activation of larger SPIs at higher temperatures can modify this trend, potentially leading to qualitatively different temperature dependence of the effective susceptibility.

These considerations are particularly relevant in environments where dust is exposed to strong radiation fields in which not only dust temperature but grain angular frequency can be increased by RATs. High-spatial-resolution polarization observations now can probe warm/hot dust in photodissociation regions, e.g., by SOFIA/HWAC+ (L. N. Tram et al. 2021; T. D. Hoang et al. 2022; N. B. Ngoc et al. 2024), active galactic nuclei (E. Lopez-Rodriguez et al. 2020), supernova ejecta (J. Rho et al. 2022), and massive star-forming regions by ALMA (P. C. Cortés et al. 2024; P. Sanhueza et al. 2025) and protoplanetary disks (I. W. Stephens et al. 2014). In such environments, dust temperatures can reach  $T_d \gtrsim 100$ –200 K, and the magnetic response of grains may differ substantially from that in the cold ISM. Whether dust polarization reliably traces magnetic fields and how the alignment efficiency varies under these conditions depends sensitively on the temperature- and frequency-dependent magnetic susceptibility of grains (A. Lazarian & T. Hoang 2007; T. Hoang & A. Lazarian 2016a; T. Hoang et al. 2022).

T. Hoang (2025) recently generalized RAT theory to provide a unified description of grain alignment and rotational disruption across diverse astrophysical environments, highlighting the central role of radiation field and magnetic relaxation in the efficiency of alignment and disruption. In this paper, we develop a physically motivated model for the effective magnetic susceptibility of dust grains containing SPIs with a power-law size distribution. We quantify how the effective susceptibility depends on dust temperature and grain angular frequency, identify the characteristic inclusion size that dominates the magnetic response, and derive analytic expressions for the resulting frequency spectrum. We then explore the implications of this effective superparamagnetism for magnetic grain alignment and magnetic dipole emission across diverse astrophysical environments.

The paper is organized as follows. Section 2 reviews the magnetic properties of paramagnetic and superparamagnetic material and discuss constraints on the maximum size of SPIs. In Section 3, we present our

model for the effective susceptibility for grains with size-distributed SPIs. Section 4 discusses the effects of effective susceptibility for grain alignment. Discussion and a summary of our main findings are shown in Section 5 and 6.

## 2. MAGNETIC PROPERTIES OF ASTROPHYSICAL DUST

In this section, we provide a brief overview of the fundamental theory concerning the magnetic properties of astrophysical dust for reference. We begin with paramagnetic and superparamagnetic dust, focusing on the case of uniform-sized SPIs, before moving on to discuss SPI size distribution in the following section.

### 2.1. Paramagnetic Dust

When iron atoms are diffusely distributed within the matrix of a dust grain, they create a standard paramagnetic material (PM). The zero-frequency susceptibility of this paramagnetic dust at temperature  $T_d$  is described by Curie's law.

$$\chi_{\text{PM}}(0) = \frac{n_p \mu^2}{3k_B T_d}, \quad (1)$$

where  $n_p$  is the number density of paramagnetic (Fe) atoms inside the dust grain, and  $\mu$  is the effective magnetic moment per iron atom  $\mu$  given by

$$\mu^2 = p^2 \mu_B^2 = g_e^2 \mu_B^2 [j(j+1)], \quad (2)$$

with  $j$  being the angular momentum quantum number of electrons in the outer partially filled shell, and  $p \approx 5.5$  is taken for silicate (see B. T. Draine 1996).

Plugging the typical numerical values into Equation (1), we obtain

$$\chi_{\text{PM}}(0) \simeq 0.03 f_p \hat{n}_{23} \left( \frac{p}{5.5} \right)^2 \left( \frac{20 \text{ K}}{T_d} \right), \quad (3)$$

where  $\hat{n}_{23} = n/10^{23} \text{ cm}^{-3}$  is the normalized density,  $f_p = n_p/n$  is the fraction of Fe atoms in the matrix of silicate grains with  $f_p = 1/7$  for silicate of structure  $\text{MgFeSiO}_4$ .

### 2.2. Superparamagnetic Dust

Iron particles (including metallic (Fe) and iron oxide particles) at low temperatures tend to be ferromagnetic in which the exchange interaction between electron spins (magnetic dipoles) enables them to be spontaneously aligned in an easy axis (e.g, long axis) for which the crystalline anisotropy energy is minimized. This results in spontaneous magnetization  $M_s$  with  $4\pi M_s = 22000, 6400, 4780 \text{ G}$  for Fe,  $\text{Fe}_3\text{O}_4$  and  $\gamma\text{Fe}_2\text{O}_3$

(see, e.g., B. T. Draine & A. Lazarian 1999b (hereafter DL99) for more details). When the temperature exceeds some threshold, so-called blocking temperature,  $T_{\text{block}}$ , the particle becomes superparamagnetic because thermal fluctuations of the lattice exceed the energy barrier (i.e., magnetostatic energy) to randomize the individual magnetic moments, resulting in a zero net intrinsic magnetic moment.

The incorporation of iron nanoparticles (hereafter iron clusters) can substantially enhance the magnetic susceptibility of a dust grain. When the grain temperature of  $T_d > T_{\text{block}}$ , the magnetic moments of single-domain clusters within the grain fluctuate rapidly, and the composite grain behaves as a superparamagnetic material (SPM). Let  $N_{\text{cl}}$  denote the number of structural formula units of the magnetic material (i.e., Fe,  $\text{Fe}_2\text{O}_3$ , or  $\text{Fe}_3\text{O}_4$ ) contained in a superparamagnetic cluster. For a metallic Fe cluster of spherical shape and radius  $r$  with mass density  $\rho = 7.86 \text{ g cm}^{-3}$ ,  $N_{\text{cl}} = (4\pi/3)r^3 \rho / m_{\text{Fe}} \simeq 355r^3$  with  $r_{-7} = r/10^{-7} \text{ cm}$ .

### 2.3. Magnetic Susceptibility for Grains with Uniform SPIs

For magnetic materials, the response of the magnetization  $M(t)$  to an oscillating magnetic field is described by dynamical equations. To model the magnetic response of the ferromagnetic material, DL99 employed the Drude model with scalar susceptibility, in which the magnetic response to the oscillating field  $H(t)$  is described by

$$\ddot{M}(t) = \omega_0^2 [\chi(0)H(t) - M(t)] - \frac{\dot{M}(t)}{\tau_0}, \quad (4)$$

where  $\chi(0)$  is the magnetic susceptibility at zero frequency,  $\omega_0$  is the resonance angular velocity (or frequency) which is defined as the precession frequency of an electron in the internal field of  $B_{\text{int}} = 4\pi M_s/3$ , i.e.,  $\omega_0 = (eB_{\text{int}}/m_e c)$  and  $\tau_0$  is the characteristic magnetic relaxation (damping) time.

The complex magnetic susceptibility is described by  $\chi(\omega) = \chi_1(\omega) + i\chi_2(\omega)$  where  $\chi_1$  and  $\chi_2$  are the real and imaginary part. The solution of Equation (4) reads (see LD99):

$$\chi_1(\omega) = \frac{\chi(0) [1 - (\omega/\omega_0)^2]}{[1 - (\omega/\omega_0)^2]^2 + (\omega\tau)^2}, \quad (5)$$

$$\chi_2(\omega) = \frac{\chi(0)\omega\tau}{[1 - (\omega/\omega_0)^2]^2 + (\omega\tau)^2}, \quad (6)$$

which depends crucially on the product  $\omega_0\tau$ . For  $\omega_0\tau < 2$ ,  $\chi(\omega)$  has the resonance near  $\omega_0$ , but the system is damped significantly for  $\omega_0\tau > 2$ . The critically damped state occurs at  $\omega_0\tau = 2$  or  $\omega_0\tau_0 = 2$ .

Assuming the critically-damped condition with  $\omega_0\tau = 2$  (DL99), the above equations become

$$\chi_1^{cd}(\omega) = \frac{\chi(0)\omega\tau [1 - (\omega\tau/2)^2]}{[1 + (\omega\tau/2)^2]^2}, \quad (7)$$

$$\chi_2^{cd}(\omega) = \frac{\chi(0)\omega\tau}{[1 + (\omega\tau/2)^2]^2}, \quad (8)$$

where  $\tau = (\omega_0^2\tau_0)^{-1}$  is the effective relaxation time, and the denominators indicate that the magnetic susceptibility is significantly suppressed when the frequency of the applied field becomes larger than the response rate of the system (i.e.,  $\omega > \omega_0 = \tau^{-1}$ ).

For our case of grains rotating at angular frequency  $\omega$ , although the grains are subject to a static interstellar magnetic field, the magnetic field appears rotating within the grain frame of reference at frequency  $\omega$ . Therefore, Equations (7-8) can be used to describe the magnetic susceptibility as a function of the grain angular frequency.

Let consider first the case of uniform SPIs having equal size of  $N_{\text{cl}}$ . In thermal equilibrium, the effective magnetic moment of the ensemble of SPIs can be described by the Langevin function with argument  $mH/k_B T_d$ , where  $m = N_{\text{cl}}\mu_0$  is the total magnetic moment of the cluster and  $\mu_0$  is the magnetic moment of basic magnetic unit (e.g., Fe atom for metallic iron), and  $H$  is the applied magnetic field (R. V. Jones & L. Spitzer 1967). Let  $\mu_0 = p\mu_B$  where  $p$  is the number of Bohr magneton per basic magnetic unit. The exact values  $p$  depends on the cluster size and it varies from  $p \sim 3$  for small metallic clusters  $N_{\text{cl}} < 100$  and saturates the the bulk metallic value of  $p \sim 2.2$  for  $N_{\text{cl}} > 500$  at  $T = 120$  K (I. M. L. Billas et al. 1994). As the temperature increases,  $p$  decreases to  $p \approx 0.5$  for  $T \sim 500 - 900$  K.<sup>3</sup>

For the case of uniform iron clusters of size  $N_{\text{cl}}$ , the composite grain exhibits superparamagnetic behavior, which has the magnetic susceptibility given by

$$\chi_{\text{SPM}}(0, N_{\text{cl}}) = \frac{n_{\text{cl}}m}{3k_B T_d}, \quad (9)$$

where  $n_{\text{cl}}$  is the volume density of iron clusters (iron clusters per unit volume).

Let  $\phi_{\text{cl}}$  be the volume filling factor of SPIs. Throughout this paper, for numerical estimates, we assume the typical value of  $\phi_{\text{cl}} = 0.03$ , i.e., about 10% of cosmic iron in the form of iron clusters (J. P. Bradley 1994; T. Hoang & A. Lazarian 2016a). Plugging  $m$  and  $n_{\text{cl}} = \mathcal{N}/V_{\text{grain}}$  with the total number of clusters

<sup>3</sup> Lower values of  $p = 1.25$  and  $1.18$  for  $\text{Fe}_2\text{O}_3$  and  $\text{Fe}_3\text{O}_4$  (see Table 1 in H. Yang (2021)).

$\mathcal{N} = \phi_{\text{cl}}V_{\text{grain}}/V_{\text{Fe}} \approx 3.5 \times 10^8 \phi_{\text{cl}} N_{\text{cl}}^{-1} a_{-5}^3$  into Equation (9), one obtains:

$$\begin{aligned} \chi_{\text{SPM}}(0, N_{\text{cl}}) &= \frac{\phi_{\text{cl}} N_{\text{cl}}}{3V_{\text{Fe}}} \frac{p^2 \mu_B^2}{k_B T}, \\ &\approx 0.1 \phi_{\text{cl}} N_{\text{cl}} \hat{p}^2 \hat{T}_d^{-1}, \end{aligned} \quad (10)$$

where  $a_{-5} = a/10^{-5}$  cm,  $\hat{p} = p/3$ , and  $\hat{T}_d \equiv T_d/15$  K.

SPIs of size  $N_{\text{cl}}$  undergo remagnetization due to thermal excitations, and the relaxation rate (aka. Néel relaxation rate) is given by (see B. T. Draine & A. Lazarian 1999a, A. H. Morrish 2001)

$$\tau_N^{-1} = \nu_0 \exp(-KV_{\text{cl}}/k_B T_d) = \nu_0 \exp(-N_{\text{cl}} T_{\text{act}}/T_d) \quad (11)$$

with  $\nu_0$  the attempt frequency,  $KV_{\text{cl}}$  the energy required for remagnetization of iron clusters of volume  $V_{\text{cl}}$ , and  $T_{\text{act}}$  is the activation temperature of superparamagnetism defined by  $T_{\text{act}} = KV_{\text{cl}}/(N_{\text{cl}}k_B)$ . For metallic Fe clusters with  $K = 1.35 \times 10^5$  erg cm<sup>-3</sup> and  $V_{\text{cl}} = N_{\text{cl}}V_{\text{Fe}} = 1.2 \times 10^{-23} N_{\text{cl}}$  cm<sup>-3</sup> where  $V_{\text{Fe}} = 1.18 \times 10^{-23}$  cm<sup>3</sup> is the atomic Fe volume, one obtains  $T_{\text{act}} = KV/(k_B V_{\text{Fe}}) = 0.011$  K. Similarly,  $\text{Fe}_2\text{O}_3$  (maghemite,  $K = 6.1 \times 10^5$  erg cm<sup>-3</sup>,  $V_{\text{Fe}_2\text{O}_3} = 7.2 \times 10^{-23}$  cm<sup>3</sup>),  $T_{\text{act}} = KV_{\text{cl}}/(k_B V_{\text{Fe}_2\text{O}_3}) = 0.32$  K. For  $\text{Fe}_3\text{O}_4$  (magnetite,  $K = 1.9 \times 10^5$  erg cm<sup>-3</sup>,  $V_{\text{Fe}_3\text{O}_4} = 7.4 \times 10^{-23}$  cm<sup>3</sup>),  $T_{\text{act}} = KV_{\text{cl}}/(k_B V_{\text{Fe}_3\text{O}_4}) = 0.1$  K. In the following, our numerical results are shown for SPIs of metallic irons, but the results can be adapted for maghemite and magnetite.

#### 2.4. Critical blocking size of SPIs determined by magnetic relaxation and gas randomization

Thermal fluctuations enable the magnetic moments of iron clusters to undergo Néel relaxation, allowing composite grains to exhibit SPM behavior. For this to influence grain alignment, the relaxation timescale,  $\tau_N$ , must be shorter than the randomization timescale due to gas collisions  $\tau_{\text{gas}}$  (see Eq. 38). If  $\tau_N > \tau_{\text{gas}}$ , grains are randomized before SPIs can relax, corresponding to the regime in which SPIs are effectively “blocked”. Because  $\tau_N$  depends on SPI size, we define the critical size above which SPIs are blocked (the critical blocking size),  $N_{\text{cri}}$ , by setting  $\tau_N = \tau_{\text{ran}}$ :

$$N_{\text{cri}} = \left( \frac{T_d}{T_{\text{act}}} \right) \ln(\nu_0 \tau_{\text{gas}}) \simeq 10^3 \left( \frac{T_d}{10 \text{ K}} \right) \ln(\nu_0 \tau_{\text{ran}}) \quad (12)$$

Using the randomization time  $\tau_{\text{gas}} \sim (8.26 \times 10^6/n_{\text{H}})$  yr (Eq. 38) and  $\nu_0 \sim 10^9$  s<sup>-1</sup>, one has  $\ln(\nu_0 \tau_{\text{gas}}) \approx 44.7, 21.7$  for  $n_{\text{H}} = 10^4$  cm<sup>-3</sup> and  $n_{\text{H}} = 10^{14}$  cm<sup>-3</sup>. The critical blocking size of SPIs is then  $N_{\text{cri}} = 4.47 \times 10^4 (T_d/10 \text{ K})$  and  $2.17 \times 10^4 (T_d/10 \text{ K})$ ,

which decreases by a factor of 2 when the density increases by 10 orders of magnitude. Therefore, dust temperature is the main parameter controlling the critical blocking size,  $N_{\text{cri}}$ .

For  $N_{\text{cl}} > N_{\text{cri}}$ , SPIs are blocked and the SPM of these clusters are zero. Therefore, the maximum susceptibility of superparamagnetic grains is given by

$$\chi_{\text{SPM}}^{\text{max}}(0) = \chi_{\text{SPM}}(0, N_{\text{cri}}), \quad (13)$$

calculated by Equation (10) in which  $N_{\text{cl}} = N_{\text{cri}}$ , corresponding to the case in which all iron clusters embedded in the grain have the same size.

### 3. EFFECTIVE MAGNETIC SUSCEPTIBILITY OF SUPERPARAMAGNETIC GRAINS

#### 3.1. Size distribution of SPIs

Here we consider a realistic case in which SPIs follow a distribution function  $f(N)$  with  $N$  the number of iron atoms per iron cluster.<sup>4</sup> The number density of SPIs with size between  $N, N + dN$  is given by the power-law distribution

$$dn = f(N)dN = CN^{-q}dN, \quad (14)$$

where  $f_N = CN^{-q}$  is the size distribution with the slope  $q > 0$ , and  $C$  is the normalization factor determined by the iron abundance in the form of iron clusters (i.e., volume filling factor  $\phi_{\text{cl}}$ ). The SPI size distribution has the lower limit  $N_{\text{min}}$  to upper limit  $N_{\text{max}}$ . The lower limit is  $N_{\text{min}} \sim 20$  (I. M. L. Billas et al. 1994), and the upper limit is determined by the upper limit for single-domain ferromagnetic material of  $N_{\text{max}} \approx 5 \times 10^5$  (E. F. Kneller & F. E. Luborsky 1963). For this paper, we consider a typical slope of  $q = 11/6$  (see Appendix A), derived from the assumption that SPIs follow the standard size distribution of interstellar dust (J. S. Mathis et al. 1977a).

$$C = \frac{(2-q)\phi_{\text{cl}}V_{\text{grain}}}{V_{\text{Fe}}N_{\text{max}}^{2-q}} \frac{1}{[1 - (N_{\text{min}}/N_{\text{max}})^{2-q}]}, \quad (15)$$

where  $V_{\text{Fe}}$  is the atomic Fe volume and  $V_{\text{grain}}$  is the grain volume.

#### 3.2. Effective magnetic susceptibility at zero-frequency

The magnetic susceptibility of SPM grains induced by iron clusters with size between  $N, N + dN$  is given by

$$d\chi(0, N) = \frac{N^2 p^2 \mu_B^2 dn}{3k_B T_d} = \frac{N^2 p^2 \mu_B^2 f(N) dN}{3k_B T_d}. \quad (16)$$

<sup>4</sup> Here,  $N \equiv N_{\text{cl}}$ , but the subscript is omitted for convenience.

We define the *effective superparamagnetic susceptibility* as the susceptibility obtained by averaging the single-particle superparamagnetic response over the size distribution of SPIs, which becomes

$$\begin{aligned} \chi_{\text{eff}}(0) &= \int_{N_{\text{min}}}^{N_{\text{max}}} d\chi(0, N) = \int_{N_{\text{min}}}^{N_{\text{max}}} \frac{p^2 \mu_B^2 N^2 f(N) dN}{3k_B T_d}, \\ &= \int_{N_{\text{min}}}^{N_{\text{max}}} \frac{C p^2 \mu_B^2 N^{2-q} dN}{3k_B T_d}, \end{aligned} \quad (17)$$

which can be rewritten as

$$\begin{aligned} \chi_{\text{eff}}(0) &= \frac{C p^2 \mu_B^2}{3kT} \int_{N_{\text{min}}}^{N_{\text{cri}}} N^{2-q} dN \\ &= \frac{C p^2 \mu_B^2}{3(3-q)kT} N_{\text{cri}}^{3-q} [1 - (N_{\text{min}}/N_{\text{cri}})^{3-q}] \end{aligned} \quad (18)$$

Using the normalization  $C$  from Equation (15), one obtains

$$\begin{aligned} \chi_{\text{eff}}(0) &= \chi_{\text{SPM}}(0, N_{\text{cri}}) \times F_{\text{eff}}, \\ &= \chi_{\text{max}}(0) \times F_{\text{eff}}, \end{aligned} \quad (19)$$

where  $\chi_{\text{max}}(0) \equiv \chi_{\text{SPM}}(0, N_{\text{cri}})$  is the maximum superparamagnetic susceptibility estimated at  $N_{\text{cl}} = N_{\text{cri}}$  given by Equation (17), and the reduction factor  $F_{\text{eff}}$  given by

$$\begin{aligned} F_{\text{eff}} &= \frac{2-q}{3-q} \left( \frac{N_{\text{cri}}}{N_{\text{max}}} \right)^{2-q} \left( \frac{1 - (N_{\text{min}}/N_{\text{cri}})^{3-q}}{1 - (N_{\text{min}}/N_{\text{max}})^{2-q}} \right), \\ &= \frac{2-q}{3-q} \left( \frac{T_d}{T_{\text{act}}} \right)^{2-q} \left( \frac{\ln(\nu_0 \tau_{\text{ran}})}{N_{\text{max}}} \right)^{2-q} \\ &\times \left( \frac{1 - (N_{\text{min}}/N_{\text{cri}})^{3-q}}{1 - (N_{\text{min}}/N_{\text{max}})^{2-q}} \right). \end{aligned} \quad (20)$$

Since  $N_{\text{min}} \ll N_{\text{max}}$  and  $N_{\text{min}} \ll N_{\text{cri}}$ , the final bracket term goes to unity. For  $q < 2$ , the reduction factor  $F_{\text{eff}}$  increases with  $N_{\text{cri}}$ . Because  $N_{\text{cri}} \sim T_d$ , the effective susceptibility varies as  $\chi_{\text{eff}}(0) \propto T_d^{3-q}/T_d \sim T_d^{2-q}$ , which increases with  $T_d$  for the standard slope of  $q = 11/6$ . This is opposite to the steep decrease as  $1/T_d$  for the single-size SPI case given by Curie law (10). The lower limit of SPIs is  $N_{\text{min}} = N_C$ , leading to the decreases of the reduction factor  $F_{\text{eff}}$  with  $T_d$ . However, as  $T_d$  increases,  $N_{\text{cri}}$  also increases, so does  $F_{\text{eff}}$  (20), so the effect of  $N_C$  on  $F_{\text{eff}}$  is subdominant.

Figure 1 (left panel) shows the rapid increase of the critical blocking SPI size with  $T_d$ , but the reduction factor  $F_{\text{eff}}$  slowly increases with  $T_d$ , spanning from 0.01–0.1 for three slopes of the SPI size distribution. It implies that larger SPIs are activated by increasing the dust temperature.

Figure 1 (right panel) shows the zero-frequency susceptibility as a function of dust temperature for different SPI sizes ( $\chi_2(0, N_{\text{cl}})$ ), the maximum susceptibility

at the critical size ( $\chi_{\text{SPM}}(0, N_{\text{cri}})$ ), and the effective susceptibility obtained by integrating over the SPI size distribution ( $\chi_{\text{eff}}(0)$ ) for the three different slopes  $q$ . The single-size susceptibility decreases with temperature as  $1/T_d$  described by Curie's law. In contrast, the maximum and effective susceptibility slightly vary with  $T_d$  due to the increase in the critical blocking size induced by stronger thermal fluctuations. For the typical slope of  $q = 11/6$ , the effective susceptibility even slightly increases with  $T_d$ , in contrast to Curie's law.

### 3.3. Rotating Grains and Resonance Size of SPIs

For a grain rotating with the angular velocity  $\omega$ , the frequency-dependence susceptibility (imaginary part) of SPIs of size  $N_{\text{cl}}$  in the critically damped condition is given by

$$\chi_2^{\text{cd}}(\omega, N_{\text{cl}}) = \frac{\chi(0)\omega\tau_N}{[1 + (\omega\tau_N/2)^2]^2}, \quad (21)$$

where  $\tau_N$  is the magnetic relaxation timescale for SPIs of size  $N_{\text{cl}}$ , as given by Equation (11). Because only the imaginary part of the magnetic susceptibility is relevant for magnetic grain alignment and magnetic dipole emission, in the following, we present the results for the imaginary part only. The theory can be straightforwardly applied to the real part.

The magnetic susceptibility  $\chi_2^{\text{cd}}(\omega, N_{\text{cl}})$  achieves its maximum at the rotation rate of  $\omega = \tau_N^{-1}$ , defined as resonance rotation rate

$$\omega_{\text{res}} = \nu_0 \exp\left(-\frac{T_{\text{act}}N_{\text{cl}}}{T_d}\right), \quad (22)$$

which corresponds to  $\omega_{\text{res}} = 1.7 \times 10^4 \text{ s}^{-1}$  for  $N_{\text{cl}} = 10^4$ , and  $\omega_{\text{res}} = 8.9 \times 10^8 \text{ s}^{-1}$  for  $N_{\text{cl}} = 100$ , assuming the same temperature of  $T_d = 10 \text{ K}$ .

For a given grain rotation rate and a SPI size, one can define the resonance temperature as

$$T_{\text{res}} = \frac{T_{\text{act}}N_{\text{cl}}}{\ln(\nu_0/\omega)}, \quad (23)$$

which increases with increasing  $N_{\text{cl}}$  and rotation rate  $\omega$ . For the large SPI of  $N_{\text{cl}} = 10^5$ , the resonance temperature is  $T_{\text{res}} = 95.5 \text{ K}$ ,  $119.4 \text{ K}$ , and  $159.2 \text{ K}$  for  $\omega = 10^4, 10^5$  and  $10^6 \text{ s}^{-1}$ , respectively. Therefore, large SPIs have a maximum susceptibility when the grain temperature reaches  $T_d \sim 100 - 150 \text{ K}$ .

For an ensemble of SPIs of different sizes embedded within the grain, we can define the size of SPIs that undergoes resonance as the SPI *resonance size*:

$$N_{\text{res}} = \frac{T_d}{T_{\text{act}}} \ln\left(\frac{\nu_0}{\omega}\right) \simeq 909.1 \left(\frac{T_d}{10 \text{ K}}\right) \ln\left(\frac{10^9 \text{ s}^{-1}}{\omega}\right) \quad (24)$$

which increases with  $T_d$  but decreases with  $\omega$ . SPIs of resonance size have dominant contribution to the susceptibility, whereas SPIs larger than  $N_{\text{res}}$  have thermal fluctuations slower than the grain rotation and have a minor contribution to the magnetic susceptibility.

The magnetic dissipation strength depends on the imaginary part of susceptibility as  $K_{\text{SPM}}(\omega, N_{\text{cl}}) = \chi_2(\omega, N_{\text{cl}})/\omega$ , which becomes:

$$K_{\text{SPM}}(\omega, N_{\text{cl}}) = \frac{\chi_{\text{SPM}}(0)\tau_N}{[1 + (\omega\tau_N/2)^2]^2} \simeq 2.6 \times 10^{-10} \hat{p}^2 N_{\text{cl}} \phi_{\text{cl}} \times \frac{k_{\text{SPM}}(\omega)}{T_d}, \quad (25)$$

where the last term denotes the dependence on  $T_d$  and the angular frequency with

$$k_{\text{SPM}}(\omega, N_{\text{cl}}) = \exp\left(\frac{N_{\text{cl}}T_{\text{act}}}{T_d}\right) \left[1 + \left(\frac{\omega\tau_N}{2}\right)^2\right]^{-2} \quad (26)$$

which increases with  $N_{\text{cl}}$  but decreases with increasing  $T_d$  and  $\omega$

For rotating grains at  $\omega < \tau_N^{-1}$ , the second term in the denominator is negligible and

$$\frac{k_{\text{SPM}}}{T_d} \sim \left(\frac{\exp(N_{\text{cl}}T_{\text{act}}/T_d)}{T_d}\right), \quad (27)$$

which is more rapid than the zero-frequency susceptibility given by Curie's law. Therefore, strong thermal fluctuations (Néel magnetic relaxation, i.e., smaller  $\tau_N$ ) act to significantly decrease the SPM susceptibility.

### 3.4. Effective magnetic susceptibility for the SPI size distribution

Here we calculate the effective susceptibility for the case of SPI size distribution. Following the similar procedure as above, the imaginary part of the magnetic susceptibility induced by iron clusters of size  $N, N + dN$  is given by

$$d\chi_2(\omega, N) = d\chi(0, N) \frac{\omega\tau_N}{[1 + (\omega\tau_N/2)^2]^2}, \quad (28)$$

where  $\tau_N$  is the relaxation time of iron clusters  $N$  from Equation (11).

The effective superparamagnetic susceptibility is given by

$$\begin{aligned} \chi_{\text{eff}}(\omega) &= \int_{N_{\text{min}}}^{N_{\text{max}}} d\chi_2(\omega, N) \\ &= \int_{N_{\text{min}}}^{N_{\text{max}}} \frac{p^2\mu_B^2}{3kT} \frac{\omega\tau_N}{[1 + (\omega\tau_N/2)^2]^2} N^2 f(N) dN \end{aligned} \quad (29)$$

which yields

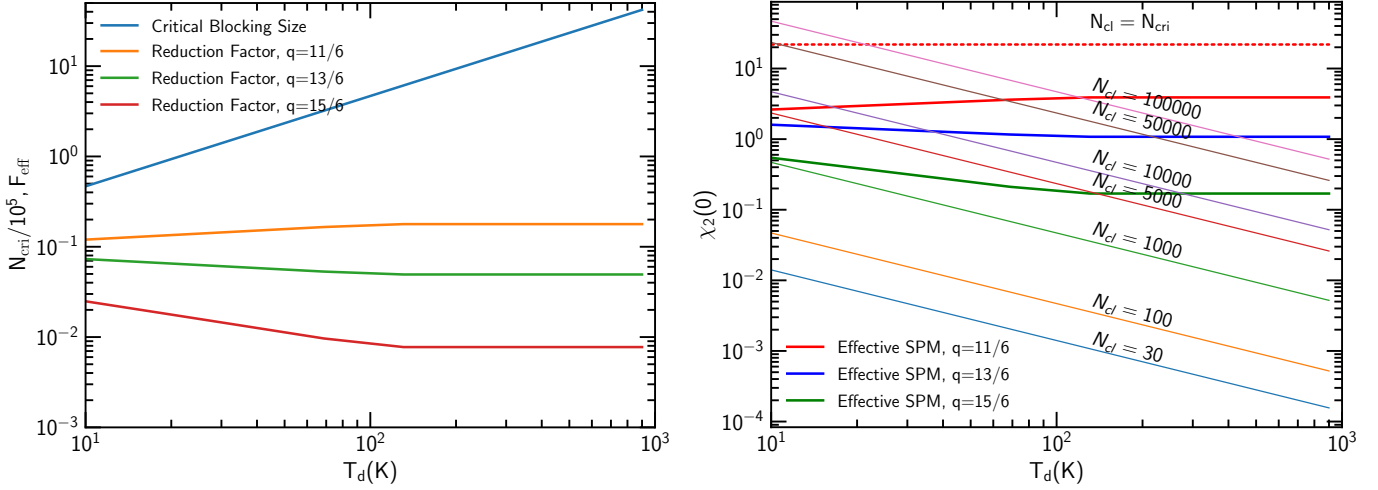


**Figure 1.** Left panel: The variation of the critical blocking size of SPIs and the effective reduction factor with  $T_d$  for the standard slope of  $q = 11/6, 13/6, 15/7$ . Right panel: The variation of the zero-frequency susceptibility with the dust temperature for the single-size SPIs compared to the effective susceptibility and the maximum susceptibility at the blocking size  $N_{\text{cri}}$ . The maximum and effective susceptibility increase with  $T_d$ , in contrast to the decrease as  $1/T_d$  for the single-size SPIs.

$$\chi_{\text{eff}}(\omega) = \frac{Cp^2\mu_B^2}{3kT} \int_{N_{\text{min}}}^{N_{\text{max}}} \frac{\omega\tau_N}{[1 + (\omega\tau_N/2)^2]^2} N^{2-q} dN \quad (30)$$

Therefore, the integral for the effective susceptibility (Eq. 30) can be evaluated with the upper limit of  $N_{\text{res}}$ , excluding the minor contribution of larger clusters ( $N > N_{\text{res}}$ ):

$$\chi_{\text{eff}}(\omega) = \frac{Cp^2\mu_B^2}{3kT} \int_{N_{\text{min}}}^{N_{\text{res}}} \omega\nu_0^{-1} e^{NT_{\text{act}}/T} N^{2-q} dN, \quad (31)$$

where the second term in the denominator is disregarded due to  $\omega\tau_N < 1$  for  $N < N_{\text{res}}$ .

One can rewrite this equation into

$$\chi_{\text{eff}}(\omega) = \frac{Cp^2\mu_B^2}{3kT} \omega\nu_0^{-1} \left( \frac{T_d}{T_{\text{act}}} \right)^{3-q} \int_{x_1}^{x_2} e^x x^{2-q} dx \quad (32)$$

where  $x = NT_{\text{act}}/T_d$ , and  $x_1 = N_{\text{min}}T_{\text{act}}/T_d$ ,  $x_2 = N_{\text{res}}T_{\text{act}}/T_d$ .

The last term can be denoted by

$$g(N_{\text{res}}) = \int_{x_1}^{x_{\text{res}}} e^x x^{2-q} dx. \quad (33)$$

which increases with  $N_{\text{res}}$  or decrease with the frequency  $\omega$  due to their relationship in Equation (24).

Finally, the effective superparamagnetic susceptibility becomes

$$\begin{aligned} \chi_{\text{eff}}(\omega) &= \frac{Cp^2\mu_B^2 N_{\text{res}}}{3kT} \omega\nu_0^{-1} N_{\text{res}}^{2-q} \ln \left( \frac{\nu_0}{\omega} \right)^{3-q} G(N_{\text{res}}) \\ &= \chi_{\text{SPM}}(0, N_{\text{res}}) \omega\nu_0^{-1} \left( \frac{N_{\text{res}}}{N_{\text{max}}} \right)^{2-q} \left( \frac{1}{1 - (N_{\text{min}}/N_{\text{max}})^{2-q}} \right) \\ &\quad \times \ln \left( \frac{\nu_0}{\omega} \right)^{q-3} g(N_{\text{res}}). \end{aligned} \quad (34)$$

The above equation can be rewritten as

$$\chi_{\text{eff}}(\omega) = \chi_{\text{SPM}}(0, N_{\text{res}}) \times G_{\text{eff}}(\omega), \quad (35)$$

where  $\chi_{\text{SPM}}(0, N_{\text{res}})$  is the zero-frequency susceptibility of single-size SPIs at the resonance size  $N_{\text{res}}$  given by Equation (10), and  $G_{\text{eff}}$  is the effective reduction factor given by

$$\begin{aligned} G_{\text{eff}}(\omega) &= \left( \frac{N_{\text{res}}}{N_{\text{max}}} \right)^{2-q} \left( \frac{1}{1 - (N_{\text{min}}/N_{\text{max}})^{2-q}} \right) \\ &\quad \times \left( \frac{\omega}{\nu_0} \right) \ln \left( \frac{\nu_0}{\omega} \right)^{q-3} g(N_{\text{res}}). \end{aligned} \quad (36)$$

Due to the weak dependence of the reduction term on  $\omega$  as the power of  $(2-q)$ , the reduction term is an order of unity. Therefore, the effective magnetic susceptibility is mostly determined by  $N_{\text{res}}$  instead of  $N_{\text{cri}}$  as in the case of grains at rest (Eq. 18). In terms of temperature with  $N_{\text{res}} \sim T_d$ , so the effective susceptibility varies as  $\chi_{\text{eff}}(\omega) \propto T_d^{3-q}/T_d \sim T_d^{2-q}$ , which increases with  $T_d$  for the standard slope of  $q = 11/6$ .

The effective superparamagnetic dissipation strength is given by

$$\begin{aligned} K_{\text{eff}}(\omega) &= \frac{\chi_{\text{eff}}(\omega)}{\omega} \\ &= \chi_{\text{SPM}}(0, N_{\text{res}}) \times \frac{G_{\text{eff}}(\omega)}{\omega}, \\ &= \chi_{\text{SPM}}(0, N_{\text{res}}) \nu_0^{-1} \ln \left( \frac{\nu_0}{\omega} \right)^{q-3} \\ &\quad \times \left( \frac{N_{\text{res}}}{N_{\text{max}}} \right)^{2-q} \left( \frac{1}{1 - (N_{\text{min}}/N_{\text{max}})^{2-q}} \right) g(N_{\text{res}}) \end{aligned} \quad (37)$$

**Table 1.** List of symbols and meaning

Notation	Meaning
$T_d$	Dust grain temperature
$\omega$	Grain rotation rate or angular frequency
$\phi_{\text{cl}}$	Volume filling factor of iron clusters inside the grain
$N_{\text{cl}}$	Number of iron atoms per cluster
$N_{\text{min}}, N_{\text{max}}$	Minimum and maximum number of iron atoms per cluster
$N_{\text{cri}}$	Critical blocking size of SPIs determined by Néel relaxation and grain randomization
$\tau_N$	Characteristic Néel relaxation timescale of SPIs by thermal fluctuations
$\chi_{\text{SPM}}(0, N_{\text{cl}})$	Zero-frequency magnetic susceptibility of the single-size SPIs
$\chi_{\text{SPM}}(\omega, N_{\text{cl}})$	Frequency-dependence superparamagnetic susceptibility for the single-size SPIs
$\chi_{\text{eff}}(\omega)$	Effective superparamagnetic susceptibility for the SPI size distribution
$K_{\text{eff}}(\omega) = \chi_{\text{eff}}(\omega)/\omega$	Effective superparamagnetic dissipation strength for the SPI size distribution
$N_{\text{res}} = T_d/T_{\text{act}} \ln(\nu_0/\omega)$	Resonance size of SPIs
$T_{\text{res}} = \frac{T_{\text{act}} N_{\text{cl}}}{\ln(\nu_0/\omega)}$	Resonance grain temperature
$\omega_{\text{res}} = \nu_0 \exp\left(-\frac{T_{\text{act}} N_{\text{cl}}}{T_d}\right)$	Resonance grain angular frequency

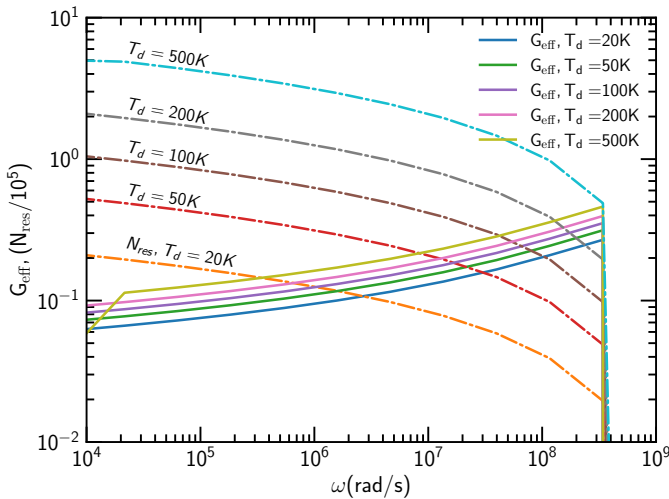


**Figure 2.** Variation of the resonance SPI size ( $N_{\text{res}}$ ) and reduction factor  $G_{\text{eff}}$  as a function of the grain rotation rate for the different dust temperature. For realistic rotation rates of  $\omega < 10^6 \text{ s}^{-1}$ ,  $N_{\text{res}}$  increases from  $10^4$  to the maximum SPI size of  $N_{\text{max}} = 5 \times 10^5$  for  $T_d$  increases from 15 K to 500 K.

where  $G_{\text{eff}}$  has been used.

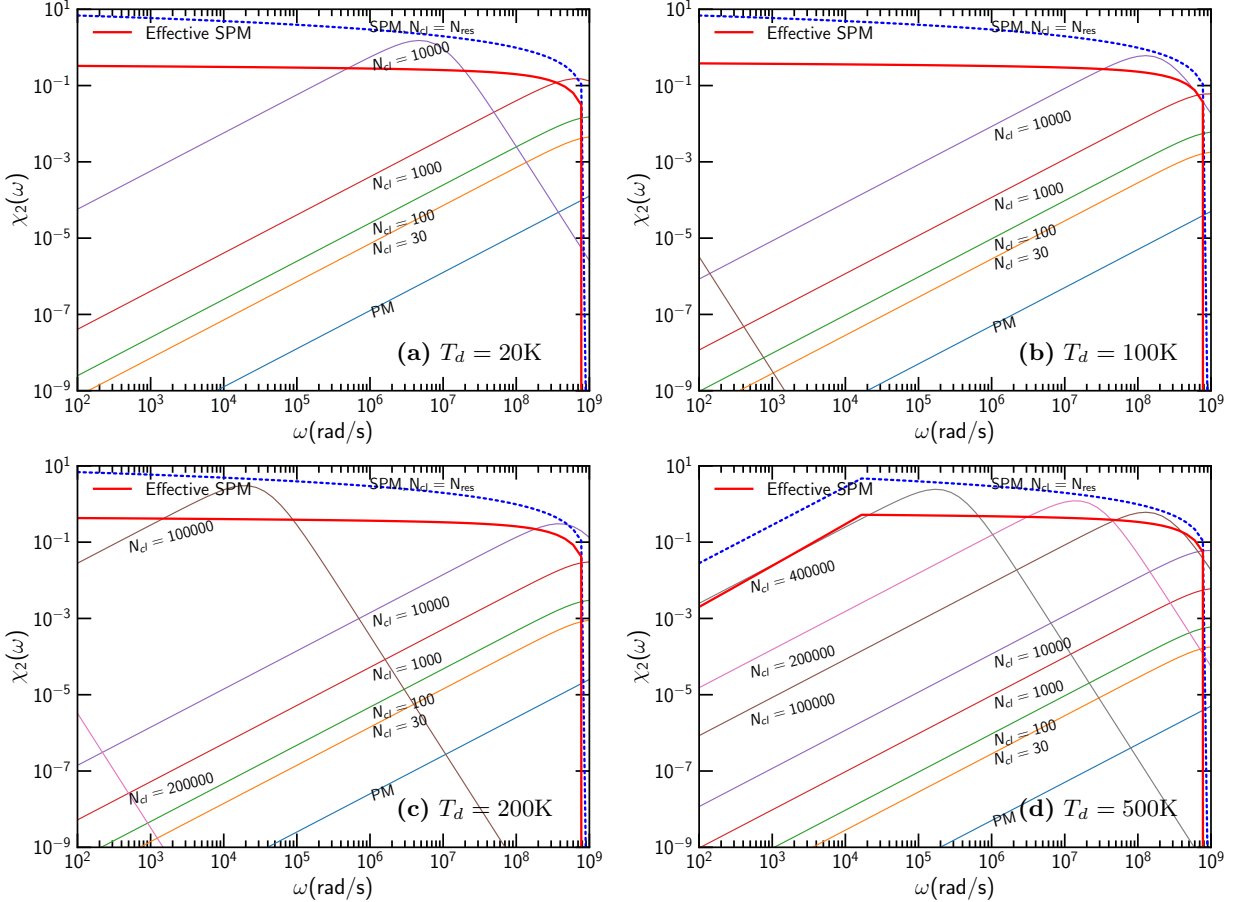
Figure 2 shows the dependence of the resonance size of SPIs,  $N_{\text{res}}$ , and the reduction factor  $G_{\text{eff}}$  on the grain rotation rate for different dust temperatures. For a fixed rotation rate,  $N_{\text{res}}$  increases with dust temperature, ranging from  $\sim 10^4$  at  $T_d = 15 \text{ K}$  to the maximum SPI size  $N_{\text{max}} = 5 \times 10^5$  at  $T_d = 900 \text{ K}$ . The reduction factor  $G_{\text{eff}}$  increases with both angular frequency and dust temperature, reflecting the enhanced contribution of thermally activated inclusions. For  $T_d < 500 \text{ K}$ ,  $G_{\text{eff}}$  typically spans the range 0.01–0.1, indicating that the effective susceptibility remains a fraction of the maximal single-size value.

Figure 3 illustrates the frequency dependence of the superparamagnetic susceptibility,  $\chi_{\text{SPM}}(\omega, N_{\text{cl}})$ , for uniform-sized SPIs at different dust temperatures. For comparison, we also show the effective susceptibility,  $\chi_{\text{eff}}(\omega)$ , obtained from the size-distribution model, as well as the paramagnetic (PM) susceptibility. For uniform-sized clusters,  $\chi_{\text{SPM}}(\omega, N_{\text{cl}})$  has the maximum at the resonance frequency  $\omega_{\text{res}}$  that shifts to lower values as the cluster size  $N_{\text{cl}}$  increases. This behavior follows from the resonance condition  $\omega_{\text{res}} \sim \tau_N^{-1} \propto \exp(-N_{\text{cl}} T_{\text{act}}/T_d)$ , indicating the exponential sensitivity of the Néel relaxation time to cluster size and temperature. In contrast, the effective susceptibility  $\chi_{\text{eff}}(\omega)$  exhibits a flat frequency dependence and remains nearly constant over a broad range of  $\omega$ , until the angular frequency approaches the characteristic attempt frequency  $\nu_0$ . This behavior arises from the superposition of resonant contributions from SPIs of different sizes.

At higher temperatures, such as  $T_d = 500 \text{ K}$ , larger SPIs become thermally activated. In this regime, the effective susceptibility increasingly resembles that of the largest active SPIs and shows a steeper decline at low rotation rates, particularly for  $\omega \lesssim 10^4 \text{ rad s}^{-1}$  (bottom-right panel).

Figure 4 shows the variation of  $\chi_{\text{SPM}}(\omega, N_{\text{cl}})$  with  $T_d$  for the different  $N_{\text{cl}}$  and at two grain angular frequencies. For the grains with single SPI size, the susceptibility has its maximum at  $T_d = T_{\text{res}}$  (Eq. 23) and decreases rapidly beyond its peak as described by  $\exp(N_{\text{cl}} T_{\text{act}}/T_d)/T_d$  (see Equation 27). However, the effective susceptibility slowly increases with  $T_d$ , resulting from the activation of larger SPIs at higher  $T_d$ .

Figure 5 shows the magnetic dissipation strength  $K(\omega, N_{\text{cl}})$  as a function of the grain angular frequency



**Figure 3.** The imaginary part of the magnetic susceptibility,  $\chi_2(\omega, N_{cl})$ , for superparamagnetic grains with uniformly sized SPIs as a function of grain rotation rate for different values of  $N_{cl}$  and dust temperatures  $T_d = 20, 50, 200, 500$  K (thin solid lines). For comparison, the maximum susceptibility at the resonance size (thin dotted line) and the effective susceptibility (thick solid line) are also plotted. As the rotation rate decreases from the characteristic  $\nu_0 = 10^9$  s<sup>-1</sup>, the peak of  $\chi_2(N_{cl}, \omega)$  shifts toward larger  $N_{cl}$  due to the resonance effect, while both the maximum and effective susceptibilities slightly increase.

for different dust temperatures. Same as the susceptibility, the magnetic susceptibility decreases by 100 times when the temperature increases from the standard value of 20 K to 150 K. The transition temperature at which the susceptibility changes from increase to decrease with  $T_d$  is determined by  $\omega > \tau_N^{-1}$  where the denominator term becomes important.

#### 4. EFFECTS OF EFFECTIVE SUPERPARAMAGNETISM ON GRAIN ALIGNMENT

Previous studies on the effect of superparamagnetism on grain alignment focus on the single-size distribution of SPIs. Our study shows the radical difference of effective superparamagnetic susceptibility obtained by averaging over the size distribution of SPIs from that of single-size SPIs. Here, we study the effects of effective magnetic susceptibility for grain alignment by deriving the essential parameters of grain alignment. Detailed modeling will be presented elsewhere.

#### 4.1. Randomization Timescale by Gas Collision and IR emission

Evaporation of gas species from the grain surface (e.g., those species that stick to the grain surface upon collisions) carries away some the grain's angular momentum and induces the damping of the grain rotation. For our numerical estimates of timescales, as in previous studies (e.g., W. G. Roberge et al. 1993), we assume the oblate spheroidal grain shape with the principal inertia moments  $I_{\parallel}$  and  $I_{\perp}$  parallel and perpendicular the symmetry axis. The characteristic timescale of the gas rotational damping is given by

$$\tau_{\text{gas}} = \frac{3}{4\sqrt{\pi}} \frac{I_{\parallel}}{1.2n_{\text{H}}m_{\text{H}}v_{\text{T}}a^4\Gamma_{\parallel}} = \frac{\sqrt{\pi}\rho_{\text{sa}}}{3n_{\text{H}}m_{\text{H}}v_{\text{T}}\Gamma_{\parallel}} \simeq 830\hat{\rho} \left( \frac{sa_{-5}}{n_4 T_{\text{gas},1}^{1/2} \Gamma_{\parallel}} \right) \text{ yr}, \quad (38)$$

where  $\hat{\rho} = \rho/(3 \text{ g cm}^{-3})$  is the normalized internal mass density of grains,  $a_{-5} = a/10^{-5} \text{ cm}$  is the normalized

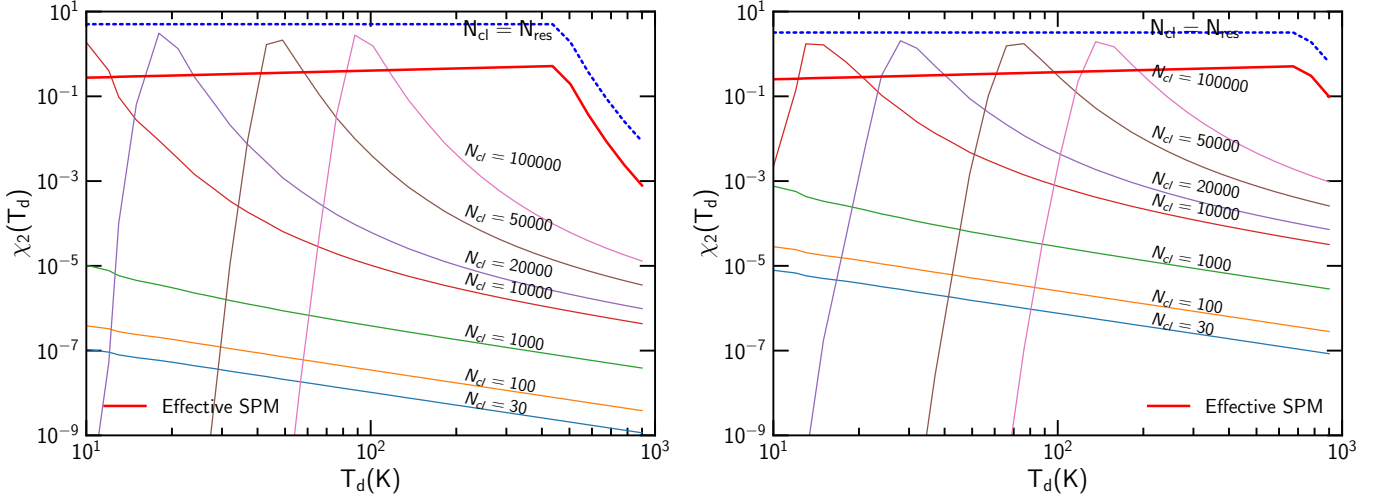


**Figure 4.** Variation of  $\chi_2(\omega, N_{cl})$  and effective susceptibility as functions of  $T_d$  for different iron clusters, assuming the grain rotation rate of  $\omega = 10^4 \text{ s}^{-1}$  (left panel) and  $10^6 \text{ s}^{-1}$  (right panel). As the temperature increases, the peak of  $\chi_2(N_{cl})$  shifts toward larger  $N_{cl}$  due to stronger thermal fluctuations. The effective susceptibility slightly increases with  $T_d$ , in contrast to the resonant behavior at  $T_d = T_{\text{res}}$  in the case of the uniform-sized SPIs.

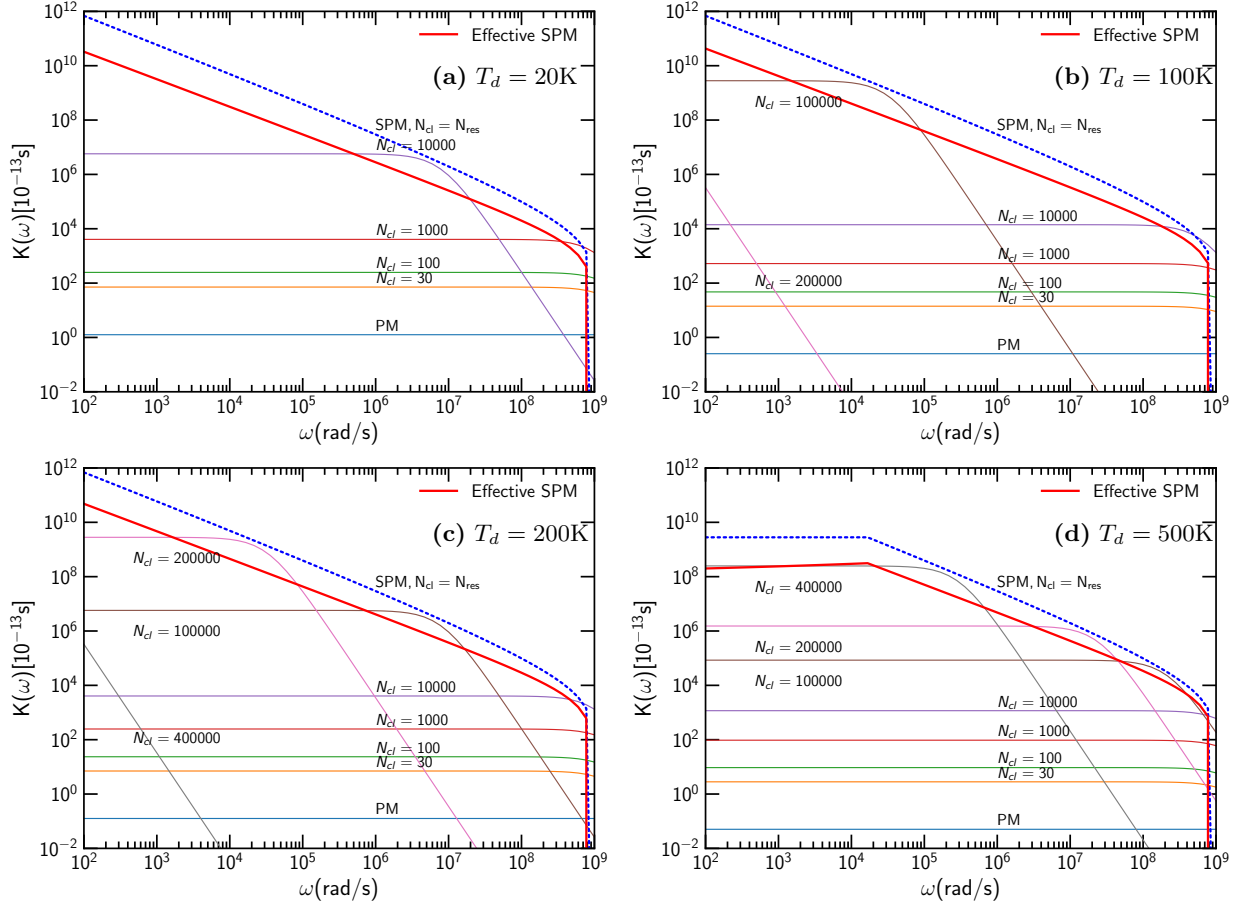


**Figure 5.** Magnetic dissipation strength  $K = \chi_2(\omega, N_{cl})/\omega$  as function of the grain angular frequencies for different dust temperatures from 20 – 500 K. The effective strength in the thick solid line is shown for comparison.

grain size,  $n_4 = n_{\text{H}}/(10^4 \text{ cm}^{-3})$ ,  $T_{\text{gas},1} = T_{\text{gas}}/10 \text{ K}$ ,  $v_T = (2kT_{\text{gas}}/m_{\text{H}})^{1/2}$ . The gas density and temperatures are normalized over the typical values of dense clouds. Above,  $s = b/a < 1$  is the ratio of the semi-minor to semi-major axes,  $I_{\parallel} = 8\pi\rho s a^5/15$  is the moment of inertia along the principal axis of maximum inertia moment, and  $\Gamma_{\parallel}$  is a geometrical parameter of order unity (W. G. Roberge et al. 1993). The gas damping time is equivalent to the timescale required for randomization of grain orientation by gas collisions.

Gas collisions lead to the thermal rotation of grains at the angular velocity

$$\omega_T = \left( \frac{kT_{\text{gas}}}{I_{\parallel}} \right)^{1/2} \simeq 3.2 \times 10^4 \text{ s}^{-1/2} a_{-5}^{-5/2} T_{\text{gas},1}^{1/2} \text{ s}^{-1} \quad (39)$$

as thermal angular momentum along the grain symmetry axis.

Subject to a radiation field of energy density  $u_{\text{rad}}$ , dust grains are heated to high temperatures and subsequently cool down by infrared (IR) emission. The IR emission also results in the rotational damping of the grain due to the loss of angular momentum carried away by photons (see B. T. Draine & A. Lazarian 1998). For a grain in thermal equilibrium of equilibrium temperature  $T_d$ , the IR damping rate is  $\tau_{\text{IR}}^{-1} = F_{\text{IR}}\tau_{\text{gas}}^{-1}$  with  $F_{\text{IR}}$  being the dimensionless IR damping parameter,

$$F_{\text{IR}} \simeq \left( \frac{3.8 \times 10^{-3}}{s^{1/3} a_{-5}} \right) \left( \frac{U^{2/3}}{n_4 T_{\text{gas},1}^{1/2}} \right), \quad (40)$$

where  $a_{\text{eff}}$  is the effective size of an irregular grain defined as the radius of an equivalent sphere of the same volume  $V_{\text{grain}} = 4\pi a_{\text{eff}}^3/3$ ,  $U = u_{\text{rad}}/u_{\text{MMP83}}$  the strength of the radiation field where  $u_{\text{MMP83}}$  is the energy density of the radiation field in the solar neighborhood from J. S. Mathis et al. (1983).

The total randomization timescale of grain alignment is

$$\tau_{\text{ran}}^{-1} = \tau_{\text{gas}}^{-1}(1 + F_{\text{IR}}), \quad (41)$$

This is the fundamental timescale that determines grain alignment against gas collisions.

#### 4.2. Barnett Magnetic Moment and Larmor Precession

A rotating magnetic grain acquires a magnetic moment through the Barnett effect (S. J. Barnett 1915). The instantaneous Barnett magnetic moment of a grain of volume  $V_{\text{grain}}$  rotating with the angular velocity  $\boldsymbol{\Omega}$  is equal to

$$\boldsymbol{\mu}_{\text{Bar}} = \frac{\chi_{\text{eff}}(0)V_{\text{grain}}\boldsymbol{\Omega}}{\gamma_g} = -\frac{\chi_{\text{eff}}(0)V_{\text{grain}}}{g_e \hbar \mu_B} \boldsymbol{\Omega}, \quad (42)$$

where  $\chi_{\text{eff}}(0)$  is the effective magnetic susceptibility of SPM grains with SPIs given by Equation (18),  $\gamma_g = -g_e \mu_B / \hbar \approx -e/(m_e c)$  is the gyromagnetic ratio of an electron,  $g_e \approx 2$  is the  $g$ -factor, and  $\mu_B = e\hbar/2m_e c \approx 9.26 \times 10^{-21} \text{ erg G}^{-1}$  is the Bohr magneton.

The period of such a Larmor precession denoted by  $\tau_{\text{Lar}}$ , is given by

$$\tau_{\text{Lar}} = \frac{2\pi}{|d\phi/dt|} = \frac{2\pi I_{\parallel} g \mu_B}{\chi_{\text{SPM}}(N_{\text{cri}}, 0) V \hbar B}. \quad (43)$$

Grain alignment occurs with respect to the magnetic field only when the Larmor precession is faster than the gas randomization. Following (T. Hoang et al. 2022), the maximum size for the grain alignment with  $\boldsymbol{J}$  aligned with the magnetic field ( $\mathbf{B}$ ) via Larmor precession, denoted by  $a_{\text{max},JB}$  (Lar) can be estimated using the condition  $\tau_B/\tau_{\text{gas}} = 1$ , yielding

$$a_{\text{max},JB}^{\text{Lar}} \simeq 5.1 \times 10^6 \left( \frac{N_{\text{cri},5} \phi_{\text{sp},-2} F_{\text{eff},-1} \hat{p}^2 B_2 \hat{s}}{n_4 T_{\text{gas},1}^{1/2} \Gamma_{\parallel}} \right) \mu\text{m}, \quad (44)$$

where  $N_{\text{cri},5} = N_{\text{cri}}/10^5$ ,  $F_{\text{eff},-1} = F_{\text{eff}}/0.1$ , and  $B_2 = B/(100\mu\text{G})$ ,

Equation (44) implies that grains are well aligned with magnetic fields in the ISM and molecular clouds because  $N_{\text{cri}} \sim 10^4 - 10^5$  (see Figure 1, left panel). In protostellar cores and disks, dust temperature can reach  $\gtrsim 100 \text{ K}$ , so  $N_{\text{cri}}$  can reach the maximum limit of  $N_{\text{max}} = 5 \times 10^5$ . Thus, very large grains of  $a \sim 5.1 \text{ mm}$  can still be aligned with the magnetic field in the protostellar envelope and hot cores/corinos of  $n_4 \sim 10^4$  (i.e. typical for protostellar cores) and  $a_{\text{max},JB}^{\text{Lar}} \sim 5.1 \mu\text{m}$  for  $n_4 \sim 10^8$  in the mid-plane of protostellar disks (T. Hoang et al. 2022).

#### 4.3. Barnett Relaxation and Internal Grain Alignment

A spinning paramagnetic grain acquires an instantaneous magnetic moment,  $\boldsymbol{\mu} \propto \boldsymbol{\Omega}$ , via the Barnett effect. The rotating magnetization component has some lag behind the grain material and induces the dissipation of the grain rotational energy, leading to the internal alignment of  $\hat{\boldsymbol{a}}_1$  with  $\boldsymbol{\Omega}$  and  $\boldsymbol{J}$  that corresponds to the minimum rotational energy state (E. M. Purcell 1979).

As shown in T. Hoang (2022), Barnett relaxation for paramagnetic grains is inefficient for large grains in dense regions like protostellar cores and disks of density  $n_{\text{H}} \gtrsim 10^6 \text{ cm}^{-3}$ . For superparamagnetic grains, the relaxation time by the Barnett effect (so-called super-Barnett relaxation) is given by

$$\begin{aligned} \tau_{\text{BR}}^{\text{SPM}} &= \frac{\gamma_e^2 I_{\parallel}^3}{V_{\text{grain}} K_{\text{eff}}(\omega) \hbar^2 (h-1) J^2} \\ &\simeq 0.16 \hat{p}^2 f(\hat{s}) a_{-5}^7 T_{d,1} \left( \frac{1}{N_{\text{res}} \phi_{\text{sp},-2} G_{\text{eff}} \hat{p}^2} \right) \left( \frac{J_d}{J} \right)^2 \end{aligned} \quad (45)$$

where  $\hat{s} = s/0.5$ ,  $h = I_{\perp}/I_{\parallel}$ ,  $f(\hat{s}) = \hat{s}[(1 + \hat{s}^2)/2]^2$ , and  $J_d = \sqrt{I_{\parallel}k_B T_d}/(h - 1)$  is the dust thermal angular momentum.

Following T. Hoang et al. (2021), we now determine the critical sizes for efficient internal alignment by super-Barnett relaxation for grains rotating with a suprathermal parameter  $St = \omega/\omega_T$ . Let  $a_{\max,aJ}$  be the maximum grain size for internal alignment between  $\hat{\mathbf{a}}_1$  and  $\mathbf{J}$ . The maximum size for efficient internal alignment by Barnett relaxation is given by  $\tau_{\text{Bar}}^{\text{SPM}}/\tau_{\text{gas}} = 1$ , yielding

$$a_{\max,aJ}(\text{BR}) \simeq 10.1 h^{1/3} St^{1/3} \left( \frac{N_{\text{res},5} \phi_{\text{sp},-2} G_{\text{eff},-1} \hat{p}^2}{\hat{\rho} n_4 T_{\text{gas},1}^{1/2} \Gamma_{\parallel}} \right)^{1/6} \times \left( \frac{(h - 1) T_{\text{gas}}}{T_d} \right)^{1/6} \mu\text{m}, \quad (46)$$

where  $G_{\text{eff},-1} = G_{\text{eff}}/0.1$ .

The above equation implies  $a_{\max,aJ}(\text{BR}) \approx 1 \mu\text{m}$  for  $N_{\text{res}} \sim 10^4$  and  $St = 1$  and  $n_4 = 1$ . One can see that  $a_{\max,aJ}$  increases with iron inclusions as  $N_{\text{cl}}^{1/6}$ , with suprathermal rotation as  $St^{1/3}$ , but decreases with the gas density as  $n_{\text{H}}^{-1/6}$  (T. Hoang et al. 2021).

Calculations in T. Hoang et al. (2021) stops at  $N_{\text{cl}} = 10^4$  due to the consideration of low temperature below which the large cluster cannot be excited, i.e.,  $N_{\text{cl}} < N_{\text{cri}}$  given by Eq. 12. However, the activation of large clusters of  $N_{\text{cl}} \sim 10^5$  in high temperatures as given by 12 can increase significantly the internal alignment size via Barnett relaxation and magnetic alignment.

Due to the significant increase of  $K_{\text{eff}}$  for SPI size distribution, Barnett relaxation becomes more efficient and can cause right internal alignment of grains with iron inclusions even at high densities. Moreover, the relaxation at lower angular velocity is faster than at higher due to the activation of larger iron inclusions.

#### 4.4. Magnetic Relaxation and Magnetically Enhanced Radiative Torque (MRAT) Alignment

Rotating magnetic (para-/superparamagnetic) grains experience the dissipation of the grain rotational energy into heat due to the lag, resulting in the alignment of  $\mathbf{J}$  with the ambient field. The relaxation time  $\tau_{\text{mag}}$  is the characteristic time of the magnetic relaxation given by

$$\tau_{\text{mag}} = \frac{I_{\parallel}}{K_{\text{eff}}(\omega) V_{\text{grain}} B^2} = \frac{2\rho a^2 s^{-2/3}}{5K_{\text{eff}}(\omega) B^2}. \quad (47)$$

To describe the aligning effect of magnetic relaxation relative to the disalignment by gas collisions, the dimensionless magnetic relaxation strength was introduced in

T. Hoang & A. Lazarian (2016a) as:

$$\delta_{\text{mag}} = \frac{\tau_{\text{gas}}}{\tau_{\text{mag}}}, \\ \simeq 948.7 \hat{\rho} a_{\text{eff},-5} \phi_{\text{sp},-2} \left( \frac{N_{\text{res},5} G_{\text{eff},-1} B_2^2}{n_4 T_1^{1/2}} \right). \quad (48)$$

The magnetic dissipation strength depends on  $T_d$  through the Curie law and the additional term determined by thermal fluctuations of SPM. In the case of single-size grains, the magnetic relaxation strength decreases with  $T_d$  due to the reduction of the magnetic susceptibility. However, for size distribution of SPIs, the maximum size increases slowly with  $T_d$ .

T. Hoang (2025) derived the critical magnetic relaxation required to produce high-J attractors for a general radiation field as

$$\delta_{\text{mag,cri}} = (1 + F_{\text{IR}}) \left[ \frac{2 - q^{\max}}{q^{\max}} \right], \quad (49)$$

where  $q^{\max}$  is the dimensionless parameter that characterizes the RAT model (A. Lazarian & T. Hoang 2007; T. Hoang & A. Lazarian 2008; J. Herranen et al. 2018).

For a strong radiation field of  $U \gg 1$  so that  $F_{\text{IR}} \gg 1$  (Eq. 40), and Equation (49) can be rewritten as

$$\delta_{\text{mag,cri}} = \frac{2 - q^{\max}}{q^{\max}} F_{\text{IR}} \quad (50)$$

$$\simeq 3.8 \frac{(2 - q^{\max})}{q^{\max}} \left( \frac{U^{2/3}}{a_{\text{eff},-5}} \right) \left( \frac{1}{n_4 T_1^{1/2}} \right), \quad (51)$$

which increases with the local radiation intensity and decreases with the gas density as  $U^{2/3}/n_4$ .

Assuming a fixed dissipation strength independent of dust temperature, which corresponds to the regime of  $T_d \gg N_{\text{cl}} T_{\text{act}}$ , T. Hoang (2025) derived the upper temperature for the MRAT effect, as given by

$$T_{\text{max}}^{\text{MRAT}} \simeq 386.2 a_{\text{eff},-5}^{1/2} \phi_{\text{sp},-2} N_{\text{res},5}^{1/4} G_{\text{eff},-1}^{1/4} B_2^{1/2} \times \left( \frac{q^{\max}}{2 - q^{\max}} \right)^{1/4} \text{K}. \quad (52)$$

As shown in Figure 2, the activation of largest SPIs at  $N_{\text{res}} = N_{\text{max}} \sim 5 \times 10^5$  at high temperature of  $T_d \sim 100 \text{ K}$  can increase the critical temperature for MRAT.

## 5. DISCUSSION

Here we apply our theory for astrophysical environments and quantify the dependence of magnetism on the distance to the source.

### 5.1. Effects of the SPI size distribution on effective superparamagnetic susceptibility

We derived the effective magnetic susceptibility of dust grains containing iron clusters by assuming a power-law size distribution of superparamagnetic inclusions (SPIs). We find that accounting for the SPI size distribution fundamentally modifies the behavior of superparamagnetic susceptibility compared to models assuming a single SPI size. At zero frequency, the effective susceptibility is primarily determined by the critical blocking size,  $N_{\text{cri}} = (T_d/T_{\text{act}}) \ln(\nu_0 \tau_{\text{ran}})$ , which corresponds to the largest SPIs that remain thermally activated over the randomization timescale. This implies that the static susceptibility is controlled by the upper end of the active size distribution rather than by a fixed characteristic inclusion size.

For rotating grains with angular velocity  $\omega$ , the effective response is dominated by a characteristic resonance size,  $N_{\text{res}} = (T_d/T_{\text{act}}) \ln(\nu_0/\omega)$ , for which the Néel relaxation time is equal to the rotational timescale. Both higher dust temperatures and slower grain rotation shift  $N_{\text{res}}$  toward larger inclusion sizes, leading to an increase in the effective susceptibility.

The frequency-dependent effective susceptibility differs qualitatively from the critically damped single-size model (Eq. 8). Instead of exhibiting a sharp resonant feature, the SPI size distribution produces a broadened response that approaches a shallow power-law behavior at frequencies below  $\nu_0$ , owing to the progressive activation of larger clusters.

Furthermore, in contrast to single-size SPI models where susceptibility decreases with increasing dust temperature due to enhanced thermal agitation, the effective susceptibility in the size-distribution model shows a slight increase with  $T_d$ . This behavior arises because higher temperatures activate larger SPIs, which contribute disproportionately to the magnetic response.

### 5.2. Physical Modeling of Grain Alignment and Polarization by the MRAT Mechanism

Superparamagnetic susceptibility plays a central role in MRAT alignment (A. Lazarian & T. Hoang 2008; T. Hoang & A. Lazarian 2016a) within the radiative torque (RAT) paradigm (T. Hoang 2025). Quantifying the efficiency of MRAT alignment therefore requires an accurate evaluation of the magnetic susceptibility. In conventional single-size SPI models, the susceptibility depends on parameters such as the characteristic cluster size  $N_{\text{cl}}$  and the volume filling factor as  $\chi_{\text{SPM}}(0) \propto \phi_{\text{sp}} N_{\text{cl}}$  (see Eq. 17). However, the adoption of a fixed  $N_{\text{cl}}$  implies the sensitive dependence of  $\chi_{\text{SPM}}$  on dust temperature  $T_d$ , since the thermal activation of

SPIs depends exponentially on  $N_{\text{cl}}$ . As a result, a single-size susceptibility model may be applicable in a limited temperature range but can significantly underestimate susceptibility in environments with higher  $T_d$ .

In contrast, our effective superparamagnetic susceptibility model, based on a size distribution of SPIs, naturally incorporates the temperature- and frequency-dependent activation of inclusions through the critical blocking size and the resonance size. For grains rotating at angular velocity  $\omega$ , the characteristic resonance size  $N_{\text{res}} = (T_d/T_{\text{act}}) \ln(\nu_0/\omega)$  determines the dominant contribution to the magnetic response.

Within the standard RAT framework, grain alignment occurs at low- $J$  and high- $J$  attractor points with angular velocities  $\omega_{\text{low-}J} \sim \omega_T$  and  $\omega_{\text{high-}J} = \omega_{\text{RAT}}$  (T. Hoang et al. 2022). Since  $\omega_{\text{low-}J} < \omega_{\text{high-}J}$ , the resonance condition implies  $N_{\text{res}}^{\text{low-}J} > N_{\text{res}}^{\text{high-}J}$  for a given radiation field and dust temperature. Consequently, low- $J$  grains activate larger SPIs and can experience enhanced magnetic relaxation relative to high- $J$  grains. This coupling between grain rotation rate, dust temperature, and inclusion size distribution introduces a physically motivated variation in alignment efficiency across environments.

In future work, we will incorporate the size-distribution-based superparamagnetism model into our publicly available codes POLARIS (S. Reissel et al. 2016; N. C. Giang et al. 2023) and DUSTPOL-PY (H. Lee et al. 2020; L. N. Tram et al. 2021) to predict polarization signatures under specific astrophysical conditions and to compare directly with observational data.

### 5.3. Towards Constraining Iron Inclusions in Dust with Polarization

Constraining the abundance of iron inclusions in interstellar dust is crucial for understanding the cosmic iron budget and the magnetic properties of dust grains. Polarization observations provide a promising avenue for such constraints, since both grain alignment efficiency and dust polarization depend sensitively on the magnetic susceptibility determined by iron inclusions, as demonstrated in our previous studies (N. C. Giang et al. 2024, 2023).

In conventional single-size SPI models, however, there exists a degeneracy between the characteristic cluster size  $N_{\text{cl}}$  and the volume filling factor  $\phi_{\text{cl}}$ , as different combinations of these parameters can yield similar magnetic susceptibilities  $\chi_{\text{SPM}}(0)$ . This degeneracy limits the ability of polarization measurements to uniquely constrain the iron content in dust.

In contrast, our size-distribution-based superparamagnetism model naturally determines the effective mag-

netic response through the critical blocking size ( $N_{\text{cri}}$ ) and the resonance size ( $N_{\text{res}}$ ), both of which are governed by dust temperature and grain rotation rate. As a result, the effective susceptibility depends primarily on the volume filling factor  $\phi_{\text{cl}}$ , reducing the degeneracy with cluster size. This framework therefore provides a physically motivated pathway to constrain the abundance of iron inclusions using multi-wavelength polarization observations.

#### 5.4. Implications for Magnetic Dipole Emission Spectrum

Thermal fluctuations of magnetic dipoles produce magnetic dipole emission (MDE) of emissivity  $j_\nu \propto \mu_2(\omega/2\pi)B_\nu(T_d)$  where  $\mu_2 = 1 + 4\pi\chi_2$  and  $B_\nu(T_d)$  is the Planck function (B. T. Draine & A. Lazarian 1999a).

In the DL99 model, the magnetic susceptibility was evaluated for uniform-sized SPIs, resulting in a resonant spectrum characterized by a peak at the Néel relaxation frequency of the inclusions. For a single inclusion size, the susceptibility exhibits a narrow resonance at a characteristic frequency  $\omega_{\text{res}} \sim \tau_N^{-1}$ , which depends exponentially on cluster size and dust temperature through the Néel relaxation time. The susceptibility decreases rapidly away from this resonance. When a power-law distribution of SPI sizes is considered, the integration over a continuous ensemble of inclusion sizes produces a superposition of individual resonant peaks. This superposition smooths the spectral response and enhances the effective susceptibility at frequencies below the characteristic attempt frequency  $\nu_0$ . As a result, instead of a sharply peaked resonance, the effective susceptibility exhibits a broadened response that approaches a power-law-like spectrum at low frequencies. A detailed modeling of magnetic dipole emission based on the new effective susceptibility will be presented in future work.

## 6. SUMMARY

We have studied the effect of a size distribution of superparamagnetic inclusions (SPIs) on the magnetic susceptibility of dust grains containing iron clusters. Our main results are summarized as follows:

- We derived the effective susceptibility by integrating over a power-law size distribution of SPIs,  $dn/dN \sim N^{-q}$ . The zero-frequency effective sus-

ceptibility is primarily determined by the critical blocking size,  $N_{\text{cri}}$ , corresponding to the largest SPI size that remains superparamagnetic under thermal fluctuations, reduced by a factor  $F_{\text{eff}} \sim 0.1$ .

- For a grain rotating at angular frequency  $\omega$ , the effective magnetic susceptibility is dominated by a characteristic resonance size,  $N_{\text{res}}$ , defined by the condition that the Néel relaxation rate  $\tau_N^{-1}$  equal the grain angular frequency. The resonance size depends on the grain rotation rate and dust temperature as  $N_{\text{res}} = (T_d/T_{\text{act}}) \ln(\nu_0/\omega)$ .
- The effective susceptibility of grains with SPIs can be described by the susceptibility of SPIs at the resonance size and a reduction factor  $G_{\text{eff}} \sim 0.1$ . It slightly changes with the angular frequency below  $\nu_0$ , in contrast to the peaky profile for the case of single-size SPIs, due to the activation of larger iron clusters at lower frequencies.
- The effective susceptibility increases slightly with dust temperature, which is opposite to the rapid decrease as  $\exp(N_{\text{cl}}T_{\text{act}}/T_d)/T_d$  predicted for single-size SPIs. This trend arises from the thermal activation of larger inclusions at higher temperatures.
- The effective susceptibility model enables us to predict the grain alignment efficiency with ambient magnetic fields within the MRAT mechanism through the critical blocking size and resonance SPI size for the different grain rotation rates and radiation fields.
- The effective susceptibility model is expected to yield a power-law spectrum of magnetic dipole emission because the latter depends on the imaginary part of the magnetic susceptibility, which would be radically different from that derived under the assumption of uniform-sized SPIs.

## ACKNOWLEDGEMENTS

T.H. acknowledges the support from the main research project from Korea Astronomy and Space Science Institute (KASI).

## REFERENCES

Barnett, S. J. 1915, Physical Review, 6, 239

Billas, I. M. L., Chatelain, A., & de Heer, W. A. 1994, Science, 265, 1682

Bradley, J. P. 1994, Science, 265, 925

Cortés, P. C., Girart, J. M., Sanhueza, P., et al. 2024, The Astrophysical Journal, 972, 115, doi: [10.3847/1538-4357/ad59a7](https://doi.org/10.3847/1538-4357/ad59a7)

Davis, L. J., & Greenstein, J. L. 1951, ApJ, 114, 206

Davoisne, C., Djouadi, Z., Leroux, H., et al. 2006, A&A, 448, L1

Djouadi, Z., Gattaccea, J., D'Hendecourt, L., et al. 2007, A&A, 468, L9

Dolginov, A. Z., & Mitrofanov, I. G. 1976, (Astronomicheskii Zhurnal, 19, 758

Draine, B. 2024, The Astrophysical Journal, 961, 103

Draine, B. T. 1996, in Astronomical Society of the Pacific Conference Series, Vol. 97, Polarimetry of the Interstellar Medium, ed. W. G. Roberge & D. C. B. Whittet, 16

Draine, B. T., & Lazarian, A. 1998, ApJ, 508, 157

Draine, B. T., & Lazarian, A. 1999a, ApJ, 512, 740

Draine, B. T., & Lazarian, A. 1999b, Astronomical Society of the Pacific Conference Series, 181, 133

Draine, B. T., & Weingartner, J. C. 1997, ApJ, 480, 633

Giang, N. C., Gouellec, V. J. M. L., Hoang, T., Maury, A. J., & Hennebelle, P. 2024, arXiv

Giang, N. C., Hoang, T., Kim, J.-G., & Tram, L. N. 2023, Monthly Notices of the Royal Astronomical Society, 520, 3788, doi: [10.1093/mnras/stad020](https://doi.org/10.1093/mnras/stad020)

Goodman, A. A., & Whittet, D. C. B. 1995, Astrophysical Journal Letters v.455, 455, L181, doi: [10.1086/309840](https://doi.org/10.1086/309840)

Hall, J. S. 1949, Science, 109, 166

Hensley, B. S., & Draine, B. T. 2023, The Astrophysical Journal, 948, 55, doi: [10.3847/1538-4357/acc4c2](https://doi.org/10.3847/1538-4357/acc4c2)

Herranen, J., Lazarian, A., & Hoang, T. 2018, arXiv:1812.07274

Hildebrand, R. H. 1988, Royal Astronomical Society, 29, 327

Hiltner, W. A. 1949, Nature, 163, 283

Hoang, T. 2019, ApJ, 876, 13

Hoang, T. 2022, ApJ, 928, 102, doi: [10.3847/1538-4357/ac5408](https://doi.org/10.3847/1538-4357/ac5408)

Hoang, T. 2025, The Astrophysical Journal, 994, 115, doi: [10.3847/1538-4357/ae0a1a](https://doi.org/10.3847/1538-4357/ae0a1a)

Hoang, T., & Lazarian, A. 2008, MNRAS, 388, 117

Hoang, T., & Lazarian, A. 2016a, ApJ, 831, 159

Hoang, T., & Lazarian, A. 2016b, The Astrophysical Journal, 821, 91, doi: [10.3847/0004-637x/821/2/91](https://doi.org/10.3847/0004-637x/821/2/91)

Hoang, T., Tram, L. N., Lee, H., & Ahn, S.-H. 2019, natas, 3, 766

Hoang, T., Tram, L. N., Lee, H., Diep, P. N., & Ngoc, N. B. 2021, ApJ, 908, 218, doi: [10.3847/1538-4357/abd54f](https://doi.org/10.3847/1538-4357/abd54f)

Hoang, T., Tram, L. N., Minh Phan, V. H., et al. 2022, AJ, 164, 248, doi: [10.3847/1538-3881/ac9af5](https://doi.org/10.3847/1538-3881/ac9af5)

Hoang, T., & Truong, B. 2024, The Astrophysical Journal, 965, 183, doi: [10.3847/1538-4357/ad2a56](https://doi.org/10.3847/1538-4357/ad2a56)

Hoang, T. D., Ngoc, N. B., Diep, P. N., et al. 2022, The Astrophysical Journal, 929, 27, doi: [10.3847/1538-4357/ac5abf](https://doi.org/10.3847/1538-4357/ac5abf)

Jenkins, E. B. 2009, ApJ, 700, 1299

Jones, R. V., & Spitzer, L. 1967, ApJ, 147, 943

Kneller, E. F., & Luborsky, F. E. 1963, Journal of Applied Physics, 34, 656

Lazarian, A. 2003, J. Quant. Spectrosc. Rad. Trans., 79, 881

Lazarian, A., Andersson, B.-G., & Hoang, T. 2015, in Polarimetry of stars and planetary systems, ed. L. Kolokolova, J. Hough, & A.-C. Levasseur-Regourd ((New York: Cambridge Univ. Press)), 81

Lazarian, A., & Hoang, T. 2007, MNRAS, 378, 910

Lazarian, A., & Hoang, T. 2008, ApJ, 676, L25

Lazarian, A., & Hoang, T. 2019, ApJ, 883, 122

Lee, H., Hoang, T., Le, N., & Cho, J. 2020, ApJ, 896, 44

Lopez-Rodriguez, E., Dowell, C. D., Jones, T. J., et al. 2020, ApJ, 888, 66

Martin, P. G. 1995, ApJ, 445, L63

Mathis, J. S. 1986, ApJ, 308, 281

Mathis, J. S., Mezger, P. G., & Panagia, N. 1983, A&A, 128, 212

Mathis, J. S., Rumpl, W., & Nordsieck, K. H. 1977a, ApJ, 217, 425

Mathis, J. S., Rumpl, W., & Nordsieck, K. H. 1977b, ApJ, 217, 425

Morrish, A. H. 2001, The Physical Principles of Magnetism (Piscataway, NJ: IEEE Press)

Ngoc, N. B., Hoang, T., Diep, P. N., & Tram, L. N. 2024, The Astrophysical Journal, 974, 118

Pattle, K., Fissel, L., Tahani, M., Liu, T., & Ntormousi, E. 2023, in Astronomical Society of the Pacific Conference Series, Vol. 534, Protostars and Planets VII, ed. S. Inutsuka, Y. Aikawa, T. Muto, K. Tomida, & M. Tamura, 193, doi: [10.48550/arXiv.2203.11179](https://doi.org/10.48550/arXiv.2203.11179)

Planck Collaboration, Ade, P. A. R., Aghanim, N., Alina, D., & et al. 2015, A&A, 576, A104

Purcell, E. M. 1979, ApJ, 231, 404

Reissl, S., Wolf, S., & Brauer, R. 2016, A&A, 593, A87

Rho, J., Ravi, A., Chastenet, J., et al. 2022, in American Astronomical Society Meeting Abstracts, Vol. 54, American Astronomical Society Meeting Abstracts, 133.02

Roberge, W. G., Degraff, T. A., & Flaherty, J. E. 1993, ApJ, 418, 287

Sanhueza, P., Liu, J., Morii, K., et al. 2025, The Astrophysical Journal, 980, 87, doi: [10.3847/1538-4357/ad9d40](https://doi.org/10.3847/1538-4357/ad9d40)

Stephens, I. W., Looney, L. W., Kwon, W., et al. 2014, *Nature*, 514, 597

Tram, L. N., Hoang, T., Lee, H., et al. 2021, *ApJ*, 906, 115, doi: [10.3847/1538-4357/abc6fe](https://doi.org/10.3847/1538-4357/abc6fe)

Truong, B., & Hoang, T. 2025, *The Astrophysical Journal*, 981, doi: [10.3847/1538-4357/adb423](https://doi.org/10.3847/1538-4357/adb423)

Tsukamoto, Y., Maury, A., Commercon, B., et al. 2023, in *Astronomical Society of the Pacific Conference Series*, Vol. 534, *Protostars and Planets VII*, ed. S. Inutsuka, Y. Aikawa, T. Muto, K. Tomida, & M. Tamura, 317

Yang, H. 2021, *ApJ*, 911, 125, doi: [10.3847/1538-4357/abebde](https://doi.org/10.3847/1538-4357/abebde)

Ysard, N., Jones, A. P., Guillet, V., et al. 2024, arXiv

## APPENDIX

## A. SIZE DISTRIBUTION OF SPIS AND EFFECTS ON EFFECTIVE SUSCEPTIBILITY

The size distribution of SPIs is uncertain. In our study, we assumed that they follow the power-law distribution of  $dn/dN \propto N^{-q}$ . The total volume of SPIs inside a grain is calculated as

$$V_{\text{SPI}} = \int_{N_{\text{min}}}^{N_{\text{max}}} (dn/dN) NV_{\text{Fe}} dN = CV_{\text{Fe}} \int_{N_{\text{min}}}^{N_{\text{max}}} N^{-q+1} dN = \frac{CV_{\text{Fe}} N_{\text{max}}^{2-q}}{2-q} [1 - (N_{\text{min}}/N_{\text{max}})^{2-q}] \quad (\text{A1})$$

where  $NV_{\text{Fe}}$  is the volume of each cluster, and  $V_{\text{Fe}} = 1.18 \times 10^{-23} \text{ cm}^3$  is the atomic Fe volume. Using the definition of the volume filing factor of iron inclusions in the grain  $\phi_{\text{cl}} = V_{\text{SPI}}/V_{\text{grain}}$ , one obtains

$$C = \frac{(2-q)\phi_{\text{cl}}V_{\text{grain}}}{V_{\text{Fe}} [N_{\text{max}}^{2-q} - N_{\text{min}}^{2-q}]} \quad (\text{A2})$$

The slope of SPI size distribution  $q$  is uncertain. Here, we discuss the relationship between this power-law SPI distribution with the grain size distribution of interstellar dust. The size distribution of interstellar dust is usually described by a power-law

$$\frac{dn}{dr} \propto r^{-\alpha}, \quad (\text{A3})$$

where  $\alpha = 3.5$  is the standard MRN distribution [J. S. Mathis et al. \(1977b\)](#).

Because  $N_{\text{cl}} \sim r^3$ , one obtains

$$\begin{aligned} \frac{dn}{dN} &= \left( \frac{dn}{dr} \right) \left( \frac{dr}{dN} \right), \\ &\propto r^{-(\alpha+2)} \sim N_{\text{cl}}^{-(\alpha+2)/3} \end{aligned} \quad (\text{A4})$$

which yields  $q = (\alpha+2)/3$ . If SPIs follow the standard MRN distribution slope of  $\alpha = 3.5$ , then  $q = 11/6 < 2$ .

For the typical MRN slope of  $q = 11/6$ , the total volume of SPIs is determined by largest SPIs. However, if SPIs have a steeper slope of  $q > 2$ , the SPI mass is dominated by smallest clusters of  $N_{\text{min}}$ .

The slope of SPI size distribution also has important implications for the effective susceptibility. From Equation (19), one can see that for the slope of  $q < 3$  ( $\alpha < 7$ ),  $\chi_{\text{eff}}(0)$  is dominated by large SPIs, but for the rather steep slope of  $q > 3$  ( $\alpha > 7$ ), it is dominated by smallest SPIs of size  $N_{\text{min}}$ . However, the scenario with such an extreme steep slope of the SPI radius distribution of  $\alpha > 7$  is unlikely because due to grain growth and destruction in the ISM.